Mixing Processes in a Nocturnal Low-Level Jet: An LES Study

J. CUXART AND M. A. JIMÉNEZ

Grup de Meteorologia, Departmento de Física, Universitat de les Illes Balears, Palma de Mallorca, Spain

(Manuscript received 27 February 2006, in final form 10 August 2006)

ABSTRACT

A steady-state low-level jet observed in the Stable Atmospheric Boundary Layer Experiment in Spain-1998 (SABLES-98) campaign is simulated using a large-eddy simulation model. The radiation is taken into account since its contribution to the budget of the tendency of temperature is as important as the contribution of the turbulence in the surface layer. The resulting regime is a two-layer flow separated by a change of the temperature gradient at the level of maximum speed. The upper part has turbulence originated by shear production extending up to 3 times the height of wind maximum and of the same order of magnitude as in the layer below. The jet nose is seen by the model as a decoupling layer, and the use of passive scalars allows for the inspection of the amount of transport across it, which is very small. The lower layer is very sensitive to the surface boundary conditions, but the principal patterns in the upper layer do not change significantly. The runs are compared to the observations through mean profiles, time series, and probability density functions.

1. Introduction

Although the wind near the surface is frequently light or calm at night under clear sky and weak synoptic winds, some tens of meters above the ground level (AGL) the wind speed may have supergeostrophic values. This is a phenomenon called low-level jet (LLJ) or nocturnal jet since, in many cases, it forms during the night and reaches its peak during the predawn hours. As Stull (1988) summarizes (and references therein), there are several conditions that favor the formation of the LLJ. The first proposed mechanism of the LLJs was given by Blackadar (1957), analyzing the inertial oscillation resulting from the departure from the geostrophic equilibrium within the boundary layer at the end of the day. A temperature inversion at the surface may decouple the surface winds from the winds aloft, which due to the Coriolis force turn around the geostrophic value forming a LLJ. However, other factors are also often involved in the generation of this nocturnal feature. Horizontal temperature gradients generate a variation of the geostrophic wind with height (the thermal wind) and the resulting pressure gradient can induce a LLJ. These temperature gradients can be generated by a sloping terrain (see, e.g., Lenschow et al. 1988) or by surface heterogeneities. Bonner (1968) suggested that the baroclinity causing the LLJ could be either of thermal or dynamical origin, the latter in this case induced by the Rocky Mountains. Whiteman et al. (1997) also consider LLJs after a cold front passage. Katabatic and nocturnal basin-scale flows, or warm offshore flows, also have similar wind and temperature profiles.

The Stable Atmospheric Boundary Layer Experiment in Spain-1998 (SABLES-98; Cuxart et al. 2000a) took place over 14 days in September 1998 at the Centro de Investigación de la Baja Atmósfera (CIBA) site on the northern Spanish plateau. This is the upper part of the Duero River basin, an elevated flat area with a radius of about 150 km and a height of about 800 m above sea level (ASL) surrounded by mountain ranges with peaks up to 2500 m ASL. Nevertheless the basin has a slight slope of about 300 m over 150 km from the northern and southern parts to the central area, where the Duero River flows from east to west. A 100-m tower was set up, which had 15 thermocouples up to 50 m, three sonic anemometers at 6, 13, and 32 m, five levels of wind speed measured at low frequency (3, 10, 20, 50, and 100 m), three levels of wind direction (10, 20, and 100 m), three more levels of temperature (10, 20, and 50 m), and two levels of moisture (3 and 20 m),

Corresponding author address: Joan Cuxart Rodamilans, Universitat de les Illes Balears, Dpt. Física, Cra. Valldemossa, km. 7.5, 07122, Palma de Mallorca, Spain.
E-mail: joan.cuxart@uib.es

DOI: 10.1175/JAS3903.1

together with a measure of the surface temperature using a radiometer and a barometer (all the heights are AGL). Captive balloons were released continuously when the synoptic pressure gradient was slack. Different static stabilities were sampled, ranging from near neutral to very stable according to Mahrt et al. (1998) classification, during the 12-h-long nights.

In most of the more stable nights, LLJs were observed, and their main features have been analyzed in Conangla and Cuxart (2006, hereafter CC2006). Basically, they consist of a flow from the east, with maximum wind speed around 8–9 m s^{-1} located somewhere between 60 and 120 m AGL. The synoptic situation located the study area near the center of a high pressure system, with a slack pressure gradient and a very weak flow from the eastern sector. The mountains surrounding the basin diverted the synoptic flow and allowed basin-scale flows to develop during the night. The inspection of the hodographs from the soundings shows a turn of the wind consistent with an inertial oscillation during the first 3 h after sunset, and then the wind direction is from the east quadrant for the rest of the night, which could be due to the baroclinity related to the sloping terrain and also the presence of locally generated katabatic or basin-scale flows. The size of the basin can also constrain the ability of the winds to continue rotating.

In CC2006, one of the observed LLJs was chosen for a more detailed study using a single-column model (described in Cuxart et al. 2000b). The main purpose was to see if the model was able to generate turbulent motions at the upper part of the LLJ (above the maximum wind speed) as the low values of the Richardson number computed from the soundings seemed to indicate. The model showed that conditions are met for turbulence mixing in that layer, basically due to shear production combined with a weak temperature gradient. An elevated layer of turbulence at a height between 1 and 3 times the height of the wind maximum (h_{LLJ}) was found, similarly to what Smedman et al. (1993) had previously indicated for a marine LLJ. Both turbulent layers were practically decoupled, as seen in the turbulence kinetic energy (TKE) budget, where near h_{LLJ} there is a layer with almost no TKE.

In this work, a similar approach will be followed but using a large-eddy simulation (LES) as the analyzing tool. The fact that the most energetic turbulent motions are explicitly resolved by the model allows for the computation of diagnostics that may complement the interpretation of the available data, taking the observed case as a guideline for the numerical experiment. The LES of the stably stratified atmospheric boundary layer (SBL) is difficult, since the stability of stratification introduces anisotropy in the process of mixing and the vertical dimension of the eddies can be very small if the stability is strong. In this case, the energetic eddies are also very small and very high resolutions would be needed.

Current available computing power restricts us to a resolution of a meter or more making it impossible to go to submeter resolutions and to keep domains large enough to represent the integral scale of the SBL (hundreds of meters). This compels the LES to be highly dependent on the details of the subgrid-scale model, since a very significant part of the turbulent motions is not resolved, especially in the most stable layer near the ground. The variability of the LES results for the SBL can be seen in Beare et al. (2006), where it seems clear that the sensitivity of the results to the subgrid scheme decreases with increasing resolution. Jiménez and Cuxart (2005) have shown that, for one particular LES model, the main features of the SBL are reproduced when compared to observational data. The largest departures are found in the surface layer, where the Monin–Obukhov similarity imposed does not seem to fit well with the data. The results were sensitive to the resolution, and runs at 3 m were closer to the data than at 5 m. The model was explored for only weak to moderate stabilities, with geostrophic forcings not lower than 5 m s^{-1}.

Here an attempt to make an LES based on an observed LLJ is made using the same model as in Jiménez and Cuxart (2005). The main interest is to describe how the turbulence mixing takes place below, across, and above the level of the wind maximum, usually coincident with a change of the temperature gradient. The observed LLJs in the SABLES-98 campaign are taken as reference. One more aim is to inspect what would be the shape and intensity of some relevant parameters for turbulence parameterization schemes, such as eddy diffusivities, mixing lengths, or turbulence Prandtl numbers.

The previous experience and the analysis of the available data strongly recommend explicitly accounting for the contribution of the radiation, in concordance with some previous studies, such as those by Garratt and Brost (1981) or André and Mahrt (1982), which found that the near-the-surface cooling is strongly influenced by the radiative divergence, especially under clear-sky nights with weak winds.

2. Modeling configuration and strategy

During the period of 14–21 September 1998, the situation over the CIBA site was of clear skies and slack pressure gradients. Every night there were LLJs devel-

oping over the area, sharing many characteristics (see Fig. 4 in CC2006). A total of 57% of the soundings during that period fulfilled the requirement that there be decreasing values of at least 1.5 m s^{-1} both upward and downward the maximum (Banta et al. 2002). The average height was 90 m AGL, with maximum wind speeds between 6 and 10 m s^{-1} and mostly blowing from the east. Here a simulation based on a stationary LLJ observed in SABLES-98 from midnight to 0200 UTC 21 September is made (local time is equal to UTC time).

The nonhydrostatic mesoscale atmospheric (Meso-NH) model (Lafore et al. 1998) is run in LES configuration (Cuxart et al. 2000b), taking a domain size of 600 m × 400 m × 800 m and using 100 × 100 × 150 grid points in the x, y, and z directions, respectively. The horizontal grid spacing is 6 m for x and 4 m for y. A horizontally anisotropic grid has been chosen to better resolve the streamwise streaklike structures present near the wall in shear-driven boundary layers. The vertical grid spacing changes with height; the first mass point is at 1 m AGL and the vertical resolution is 2 m in the first 100 m, stretched until 400 m where it is about 5 m, and stretched further until 800 m where it is about 30 m. For this simulation the anelastic equations of Lipps and Hemler (1982) are used and discretized on a finite difference scheme using the Gal-Chen and Somerville (1975) coordinate system. The turbulence scheme of Cuxart et al. (2000b) is applied, based on a TKE equation and the Deardorff (1980) length for the closure. The advection flux is a second-order centered scheme, flux corrected for the scalars.

The latitude (43°) and the roughness length (z_0 = 0.035 m) correspond to the SABLES-98 site (Cuxart et al. 2000a). The observed jet experiences a rotation coherent with an inertial oscillation in the first part of the night, but at about midnight a strong turbulence event takes place and a stationary jet sets up with constant direction and very weak surface cooling (see CC2006 and Cuxart et al. 2000a for details). It is likely that it is a jet of orographic origin from the distant mountain ranges at the south and the east of the measuring site. Therefore it is not considered necessary to start from the evening transition since there is such an abrupt change at midnight of, probably, an external origin. Many observed LLJs have heights in this range (between 50 and 150 m AGL), even in the American Great Plains (Banta et al. 2002), although those that are mostly caused by inertial oscillations tend to have heights above 200 m AGL. Many of them do not experience rotation with time, especially those related to warm outflows over a cold sea or orographically generated jets.

Since the observed LLJ is quasi-stationary between 0030 and 0200 UTC, the initial temperature and wind profiles for the LES model are taken from the 0030 UTC sounding (see Figs. 2a,b) within this period. The temporal series of the total integrated TKE (Fig. 6a) indicate that there is a strong spinup during the first 40 min of the simulation, and the regime becomes steady after that, with very little changes in the statistics after the second hour. However, this initializing procedure may generate large eddies performing too much mixing during the spinup.

Following the sensitivity studies of CC2006, the geostrophic wind is prescribed constant in time, with a value of 6 m s^{-1} below the maximum of the wind and a linear decrease above it up to 350 m, from where its value is 2 m s^{-1} until the top of the domain. CC2006 found that if a LLJ is already formed, a vertical variation of the geostrophic wind helps to maintain the shape of the profile, whereas taking a constant geostrophic wind with height tends to weaken the jet as the time advances. If the simulation is initialized at the evening, the vertical variation of the geostrophic wind is necessary in this modeling configuration to generate a jet.

A likely evolution of the nocturnal at low levels in the central part of the Duero basin is that the winds turn according to an inertial oscillation during the first part of the night and, afterward, a combination of katabatic flows and their interaction at the basin scale (as in Cuxart et al. 2007) sets a quasi-steady configuration at the basin scale, with little change of direction with time. The basin-scale baroclinity might also play an important role. The tests on the forcings have shown that the inner dynamics of the jet can be mimicked using a vertical variation of the geostrophic wind consistent with the thermal wind associated with the climatologically observed temperature difference across the northern Duero basin. No equivalent thermal forcing has been used. A small random perturbation is added to all velocity components to initiate the resolved motions.

Initially, the wind has a maximum of 8.8 m s^{-1} at 62 m and values near 2 m s^{-1} above 300 m, whereas the potential temperature near the ground is 286 K and has a vertical gradient of about 0.09 K m^{-1} below the wind maximum and 0.01 K m^{-1} above it. The relative humidity is below 55% all night, with the specific humidity at about 6.5 g kg^{-1}, well mixed below the jet nose. The moisture is not taken into account in this simulation, although a detailed study of its effects is planned. Nevertheless, a test using moisture does not significantly change the results in this case, since the moisture is well mixed and the flux at the surface is very small.

The radiation scheme of Morcrette (1990) is used. It calculates the radiative fluxes taking into account absorption emission of longwave radiation and reflection and scattering and absorption of solar radiation by the earth's atmosphere and surfaces. Here only the longwave part is active in a dry and clean atmosphere. The package is called every minute using the average column of the LES as input, and the obtained radiative forcing is applied at every time step for every column within the domain.

The radiative contribution is extremely important in the simulation of the clear-sky stable ABL. Räisänen (1996) shows that variations in the simulated profile of the temperature near the ground led to significant differences in the computations of the radiative cooling in this layer. Therefore, very fine resolutions near the ground must be used to try to minimize this effect. This strong temperature gradient implies a large radiative cooling rate, which is partially compensated by the turbulence mixing. Above the surface layer, the radiative cooling becomes fairly independent of the height above the ground and is only about a 20% of the turbulence contribution (Tjemkes and Duynkerke 1989).

This is the behavior found in the present simulation, as shown in Fig. 1, where the modeled contributions are compared to estimations from the observations of the studied night. The values and the profiles are very similar to the ones studied in Ha and Mahrt (2003) using data from the 1999 Cooperative Atmosphere–Surface Exchange Study (CASES-99) campaign (Poulos et al. 2002). As in Gopalakrishnan et al. (1998), here the radiative cooling is an important mechanism in the surface layer, whereas the turbulence cooling is larger above it and until the wind maximum, and, over the jet, both contributions are comparable. A test with moisture did not significantly change the results, since the actual values of the upward and downward fluxes were altered, but the vertical divergence of the total flux was almost the same.

To allow feedbacks between the soil and the atmosphere, a very simple energy balance equation (Van de Wiel et al. 2002) has been considered, where the three terms that balance are the turbulent heat flux, the flux from the soil, and the longwave radiative flux. This method has already been tested in Jiménez and Cuxart (2005) keeping the same values for the physiographical parameters. From this energy balance equation, the averaged surface vertical flux converges to about -0.010 K m s^{-1} at 2 m, larger than the one measured during the stationary period (-0.005 K m s^{-1}) at 6 m; this stronger cooling flux sustained during 4 h leads to a smaller surface temperature than the observed one at the end of the run. Tests made using different surface boundary conditions, such as prescribing the observed surface values (see below), can significantly vary the profiles within the layer below the wind maximum. Derbyshire (1990) showed that the stable limit of the surface vertical temperature flux depends on the critical Richardson number and the geostrophic wind, among other parameters. The simulated conditions are well within the range of observable conditions following Derbyshire, where the maximum value for the surface flux is -0.015 K m s^{-1}, assuming a critical Richardson number of 0.25.

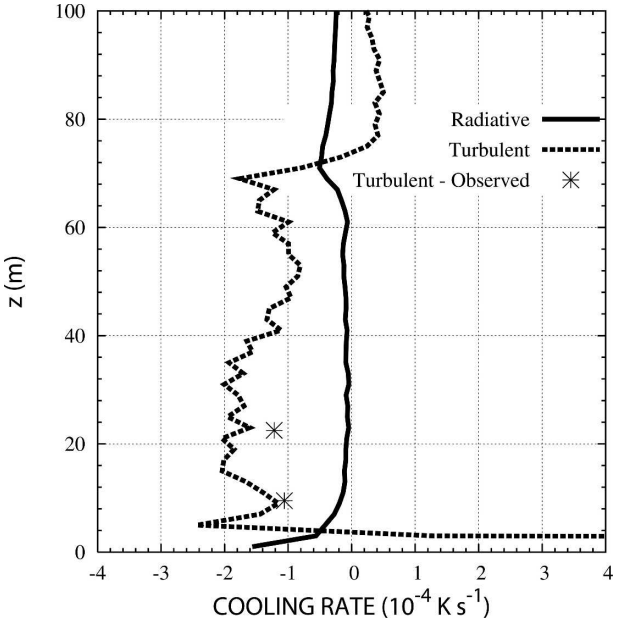

FIG. 1. Radiative $[(1/\rho C_p)(dR_{\mathrm{net}}/dz)]$ and turbulent $(d\langle w\theta\rangle/dz)$ coolings computed from the LES (in lines) and from the observations (points) between 0000 and 0200 UTC.

The run lasts 4 h and horizontal half-hourly averages are taken. One hour after the start, when the spinup is over, two scalars are introduced, one below (S_1) and one above (S_2) the wind maximum. They are used to inspect the mixing above, below, and across the LLJ maximum, as in the Wyngaard and Brost (1984) top-down and bottom-up transport in a convective boundary layer.

3. Description of the mean state and the turbulence statistics

The observed LLJ is quasi-stationary between 0000 and 0200 UTC, since the maximum wind speed is located between 55 and 80 m, with values from 8.4 to 9.2 m s^{-1}. The height of the maximum does not vary monotonically (70 m at 0030 UTC, 80 m at 0100 UTC, 60 m at 0130 UTC, and 55 m at 02000 UTC). Above the jet,

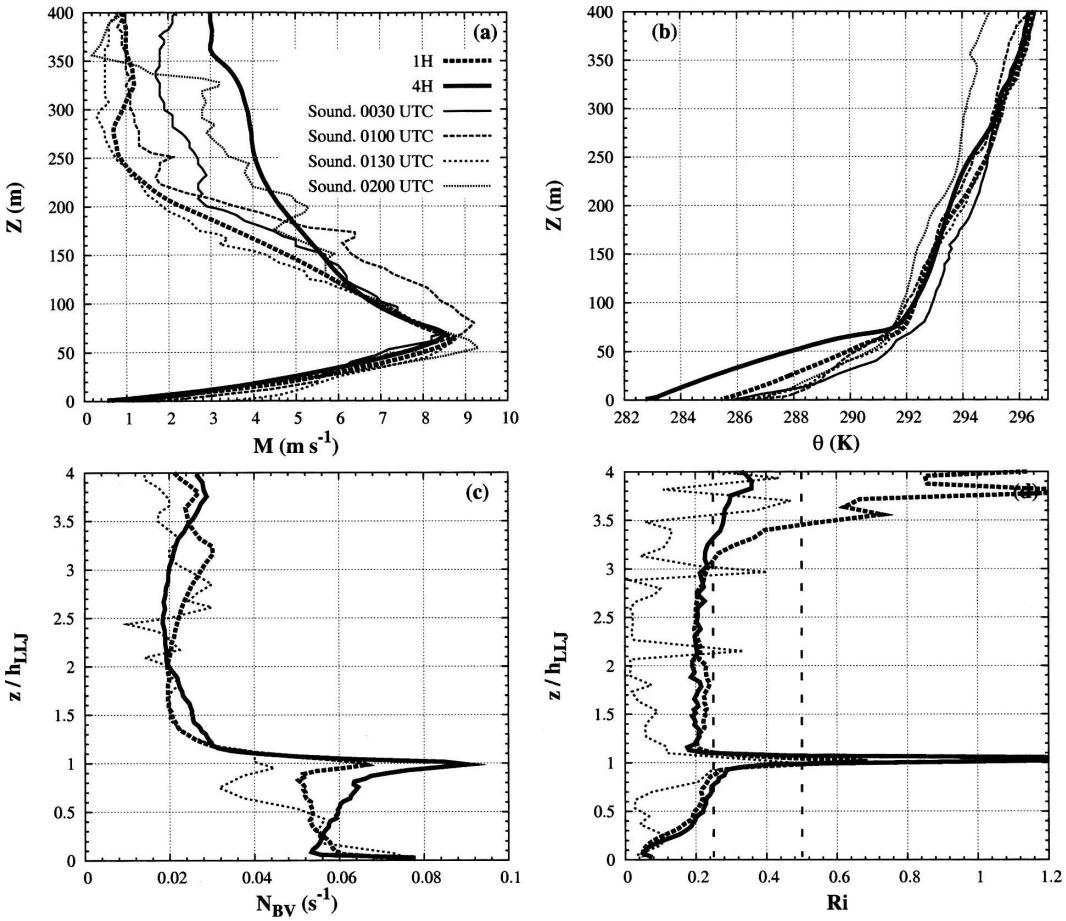

FIG. 2. Half-hourly averaged LES outputs at 1 h (thick continuous line) and 4 h (thick dashed line) and some soundings (thin lines) for (a) wind speed; (b) potential temperature; (c) Brunt–Väisälä frequency; and (d) gradient Richardson number. In (c), (d) only the 0130 UTC sounding is plotted and the y axis is normalized by the LLJ height (h_{LLJ}).

the wind speed tends to decrease with time, but there is an acceleration observed between 0130 and 0200 UTC. During this time interval, the direction varies but does not follow any well-defined pattern of rotation.

There is a change of the temperature gradient very close to the jet nose (Fig. 2a) that, depending on the sounding, can be located above or below the nose. The potential temperature profile is three layered, with a strong gradient close to the ground (2 K in the first ten meters), a weaker gradient up to the jet nose (about 4 K in fifty meters) with varying slopes, and a slack gradient above [1 K $(100\ \mathrm{m})^{-1}$] with a sudden heating on the column between 0130 and 0200 UTC. There seems to be some warm advection that has not been taken into account in the simulation and it could explain why the model is cooling too much compared to the observations.

The simulation is able to reproduce many of the relevant features, such as the height and intensity of the jet and the shear from the nose to the ground. However, the simulation shows a monotonic increase of the height of the nose from 65 to 71 m, unlike the observed evolution described above. Above the nose, the simulated wind experiences a rotation similar to the inertial oscillation, although slightly slowed down by the weak turbulence mixing above the jet, as will be described below. The soundings do not rotate in the same way, indicating that the setup misses some external forcing or a stronger elevated turbulence.

The potential temperature provided by the simulation compares well with the observations above the nose but tends to diverge from them below. The simulation completely misses the very strongly stratified layer near the ground and cools all the layers below the nose, allowing the shear to generate more turbulence that can reach the ground. This effect accumulates during the whole simulation resulting in a final profile 2 K too cold in the surface layer. Some sensitivity tests on

this point will be described later, but none manages to provide the correct curvature of the potential temperature below the nose. The layer where the temperature gradient changes is well captured, and there is also a vertical displacement in respect to the nose, similarly to the observations but with the height of this layer only about 2 m below the nose.

A number of factors can explain the problems of the simulation reproducing the thermal structure of the subjet layer. The initializing procedure might mix in excess temperature or generate too-large eddies that are not dissipated fast enough. The fact that the budget equation provides a larger cooling rate than observed might be explained by a missed warm advection. If the observed flow corresponds to a katabatic flow coming from the distant mountains, as some mesoscale simulations seem to indicate (A. Mira 2006, personal communication), the flow would not be significantly cooled by the surface (as in Cuxart et al. 2007) and this effect is not considered in this exercise. The fact that the three-layered structure is destroyed can be related to the excess of mixing in the subjet layer or to a too-coarse resolution in the surface layer that does not allow the radiation to decouple the near-the-ground air. Another test imposing the observed cooling rate (not shown) also has the wrong potential temperature curvature below the nose. The study of the thermal structure deserves further work.

The estimated Brunt–Väisälä frequency from the soundings has a maximum near the ground and a secondary one at the jet nose, diminishing strongly above it. These features are well captured by the model, as is the gradient Richardson number, where the soundings and the simulation show values below 0.25 for all the column except at the jet nose. Equivalent results were found in Mahrt et al. (1979) from sounding measurements. Interestingly, the simulation has larger Ri above the jet than the soundings, which would indicate that the real flow could have more intensity of turbulence above than the simulation. If one computes bulk parameters following Banta et al. (2003), the values for the subjet mean shear (0.12 s^{-1}), mean gradient (0.1 K m^{-1}), and flux Richardson number (0.22) are comparable to the values those authors computed for several nights of the CASES-99 campaign.

Some turbulence moments are shown in Fig. 3. They all share a two-layered structure with minimum intensity at the nose. At this level, the heat flux (both resolved and subgrid) is very close to zero, indicating that, in average, there is a very small transport of heat between the layers as seen in the 30-min averages. This does not exclude, as we will see later, that the mixing can take place in short episodes, wiped away by the averaging procedure. The comparison to fluxes computed from the sonic anemometers indicates that the model tends to overestimate the flux in the lower layer, but nothing can be said of what happens at the level of the nose and above. The soil flux computed by the energy budget equation compares very well to the observations [about 12 W m^{-2} (not shown)].

The TKE shows significant values at the jet nose level, all resolved and mostly (but not all) attributable to the resolved horizontal variances (not shown). The values below the nose are well captured although the slight increase with height is missing. Above the nose, the TKE is of the same order of magnitude as below, with a maximum at near 3 times the height of the nose consistent with the observations of Smedman et al. (1993) for a jet over the Baltic Sea or in CC2006 for this same site. The inspection of the TKE budget (Fig. 3d) shows that, even if the production of turbulence by shear is less in the upper layer, the destruction by buoyancy is stronger in the lower layer allowing for similar values for the TKE. The shear production seems somewhat overestimated in the surface, since the momentum fluxes (Fig. 3c) are too strong; this might explain the destruction of the very strongly stratified layer near the surface due to an excess of production of turbulence. The observed TKE increases with height in the subjet layer, indicating that the mixing can be "upside-down" as suggested by Mahrt et al. (1998), but it is unclear whether this turbulence comes from above the nose or if it is generated at the upper part of this layer.

The LES of stably stratified flows has difficulties in producing an inertial subrange, because the stratification acts at very small scales, introducing anisotropy at the Ozmidov scale ($L_{oz} = \sqrt{\epsilon/N^3}$), which in the present simulation is about 4 m decreasing to the centimeter scale at the very stable layer near the jet nose. Four meters are just the resolvable scale with the present resolution and the inertial subrange is not captured properly in this simulation, although the model manages to dissipate the energy through the subgrid scheme. The crosswind spectra (Fig. 4) seem to show the existence of a buoyancy subrange for all the plotted levels in a physical range up to a scale of 40 m.

4. Sensitivity tests

a. The surface layer

Figures 2 and 3 show that the model is not capturing the main features of the surface, where large gradients of temperature exist in the first meters. By default, the model prescribes the Monin–Obukhov theory for the

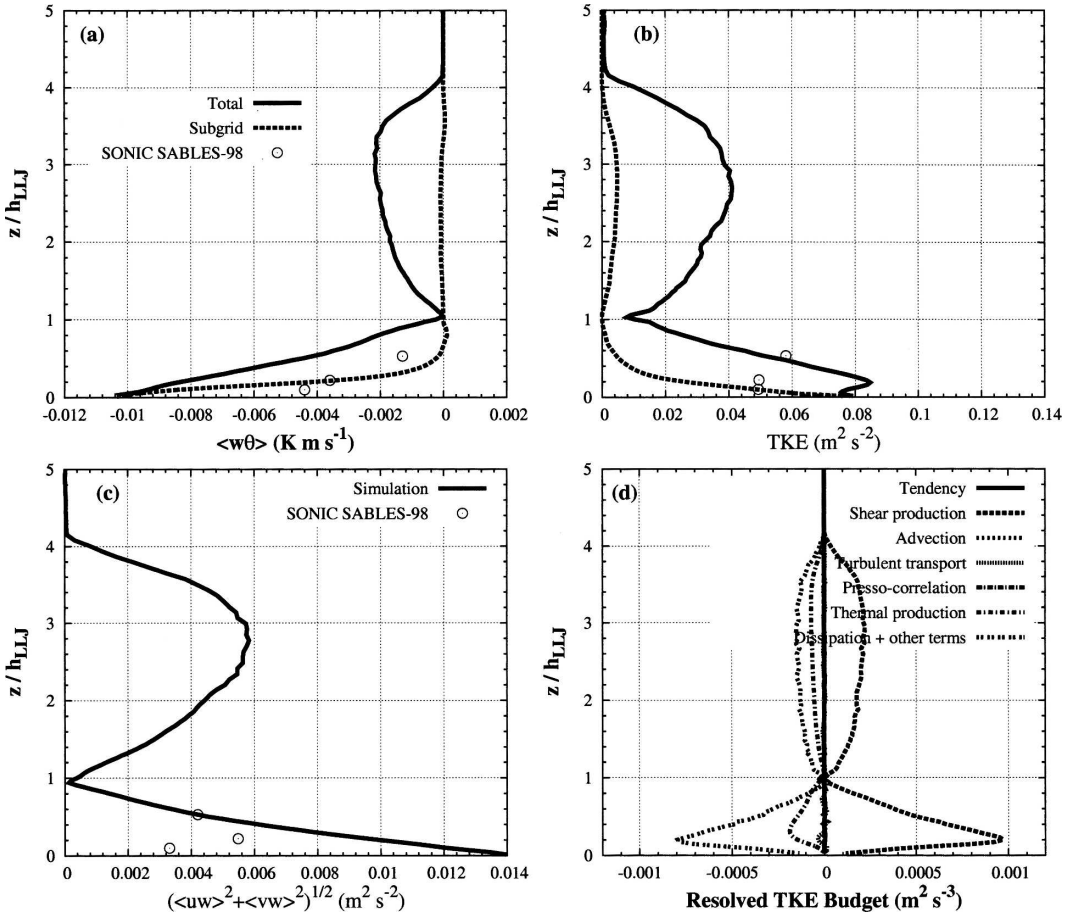

FIG. 3. Averaged LES outputs at 4 h: (a) heat flux; (b) TKE; (c) horizontal part of the Reynolds tensor; and (d) resolved TKE budget. The symbols in (a)–(c) are averages from sonic anemometers. The *y* axis is normalized by the LLJ height (h_{LLJ}).

turbulent fluxes and solves iteratively a simple energy balance equation. Apparently, with the resolution used, the model is not able to stay at almost constant values of the 2-m temperature as observed, maybe because this feature might be due to an external forcing ignored in the simulation setup, such as a very thin drainage flow or a warm advection also associated with a slope or basin-scale flow. To see if such a behavior could be imposed in the simulation, a sensitivity test is made, taking the energy budget equation using the wind and temperature at the first level of the model (1 m AGL) to be prescribed and constant, and equal to the observed average values (1.4 m s^{-1} and 286 K). This case is labeled "SURFACE" in the plots and it is made to see how working with the appropriate near-the-surface values affects the simulation results.

Even if the wind at 1 m is prescribed, the simulation tends to slow down more above the surface layer, which behaves decoupled and with a larger wind speed (Fig. 5a). The main difference is that the nose height increases with time faster than in the standard run reaching 85 m after 4 h (12 m more), although the wind speed at the nose is slightly weaker. This might be related to the larger amount of mixing across the jet in the forced case, as will be shown later. The temperature profile manages to stay parallel to the observed one, which is an improvement compared to the standard run, but it still misses the formation of a very stable layer close to the surface. This is probably related to a too-coarse vertical resolution, since most of the observed variation takes place below 10 m, with very large changes in the radiative fluxes that cannot be captured with the resolution used (Räisänen 1996). The TKE and the heat fluxes increase significantly in the surface layer but fall to values comparable to the standard run above it. The two-layered structure is not altered, although, when the observed surface parameters are prescribed, the maximum of turbulence is shifted downward due to the normalization of height by h_{LLJ}.

It is interesting to note that when the model is run

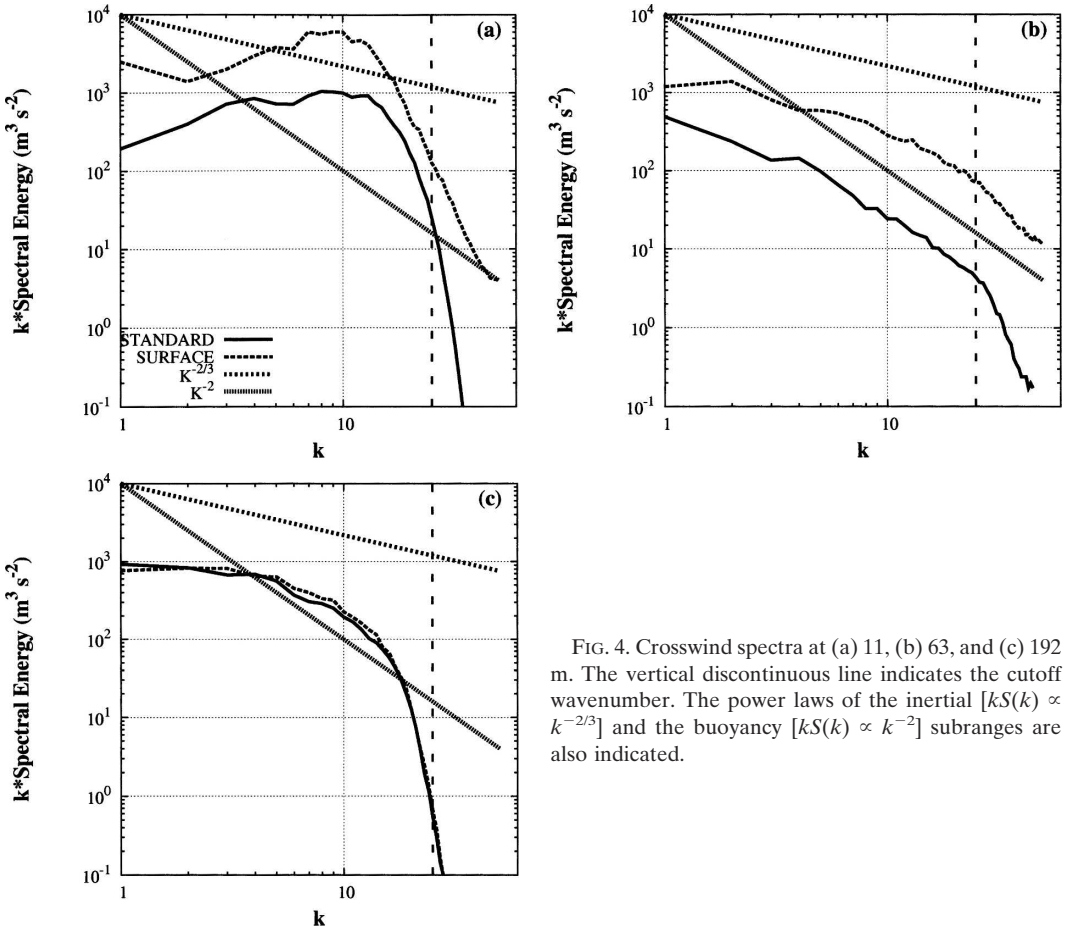

FIG. 4. Crosswind spectra at (a) 11, (b) 63, and (c) 192 m. The vertical discontinuous line indicates the cutoff wavenumber. The power laws of the inertial [$kS(k) \propto k^{-2/3}$] and the buoyancy [$kS(k) \propto k^{-2}$] subranges are also indicated.

using prescribed boundary conditions for the wind and the temperature, it experiences mixing episodes with a certain regularity as the vertically integrated resolved TKE shows (Fig. 6a). Figure 6b shows one observed mixing event during the same night (but prior to the simulated period) that has similar intensity and duration as the events produced in the simulation. This does not imply that the generating mechanism is the same but probably that the response to a forcing of the same intensity is well captured by the model. A direct comparison of three observed and simulated levels (Fig. 7a) has a similar qualitative and quantitative evolution, with larger values at 13 m rather than at 6 or 32 m.

The evolution at a very short time scale of the TKE profiles (Fig. 7b) shows that there is a sudden increase of TKE above the surface layer, reaching values up to 0.4 $m^2 s^{-2}$, followed by a jump that transports TKE upward, crossing the jet nose, and decreasing afterward. It looks like a threshold on shear is reached between the surface layer and the subjet layer, which allows for a burst of turbulence that is able to perform transport across the jet nose for a short interval. The evolution of the potential temperature in the subjet layer (Fig. 7c) shows that there is a mixing episode restricted into that layer that finally connects both layers at about 12 300 s resulting in a colder layer above the jet. This means that transport has been made across the jet nose in this modeling configuration in quite a sudden manner.

The origins of these oscillations in the observations are still unclear and deserve further investigation. Some theories propose that, near the ground, the oscillatory regime is reached for a certain range of dynamic and radiative forcings, the so-called intermittent regime (Van de Wiel et al. 2002), but these turbulence bursts are not necessarily periodic. The "Businger mechanism" (Businger 1973) is thought to explain this process. It states that the strong stratification decouples the surface layer from the flow above until a critical Richardson number is reached that allows a mixing event to take place. The surface cooling stratifies the layer again and the process starts again. This is what seems to be taking place in the surface-forced sensitivity test and does not happen in the standard configuration.

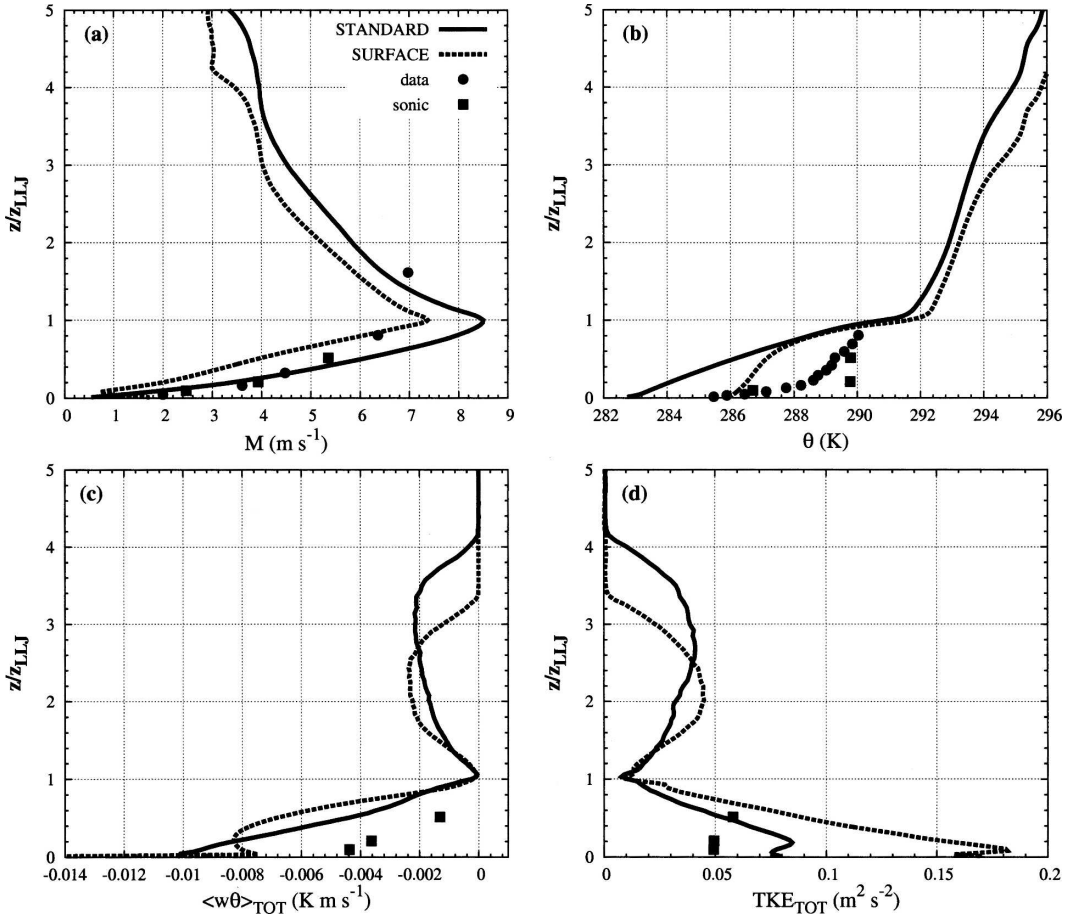

FIG. 5. Sensitivity tests: the standard case shown in Figs. 2 and 3 and the same run imposing the observed temperature and wind speed at the first computation level (labeled as surface). (a) Wind speed; (b) potential temperature; (c) heat flux; and (d) TKE. Data from the tower are shown by filled circles and measurements taken from the sonics are shown by filled squares. The y axis is normalized by the LLJ height (h_{LLJ}) obtained for each case.

b. Other sensitivities

Some other tests have been performed to see how the main results are altered if some of the key parameters of the simulation are changed. If the resolution is degraded to 5 m, there is more transport across the jet nose, although this could also be attributed to the advection scheme. This is consistent with the findings of the first Global Energy and Water Cycle Experiment (GEWEX) Atmospheric Boundary Layer Studies (GABLS) intercomparison exercise (Beare et al. 2006). If the radiation scheme is switched off, the surface temperature slightly increases because there is no radiative cooling close to the ground, although the main characteristics of the simulation do not vary much. However, finer resolution would be needed to properly capture the radiation contribution in the surface layer and to see if the differences between observations and model come from this fact. Other tests like displacing the level of change of the temperature gradient upward or downward in respect to the wind maximum (about 15 m, like the observed variability) do not alter either of the main results outlined above, that is, the two-layered structure with limited mixing across the jet nose and the wrong curvature of the potential temperature in the subjet layer.

5. Mixing across the wind maximum

Two scalars are introduced in the simulation after 1 h when the standard run has reached a steady state. A scalar (S_1) is initialized as 1 between the ground and 0.8 h_{LLJ} and another one (S_2) as 1 from 1.4 to 4.2 h_{LLJ}. Both scalars are immediately well mixed within their layer and reach the jet nose. After 4 h of simulation, a small amount of scalar has crossed this level in both senses (Fig. 8), and there is no numerical loss of scalar in the

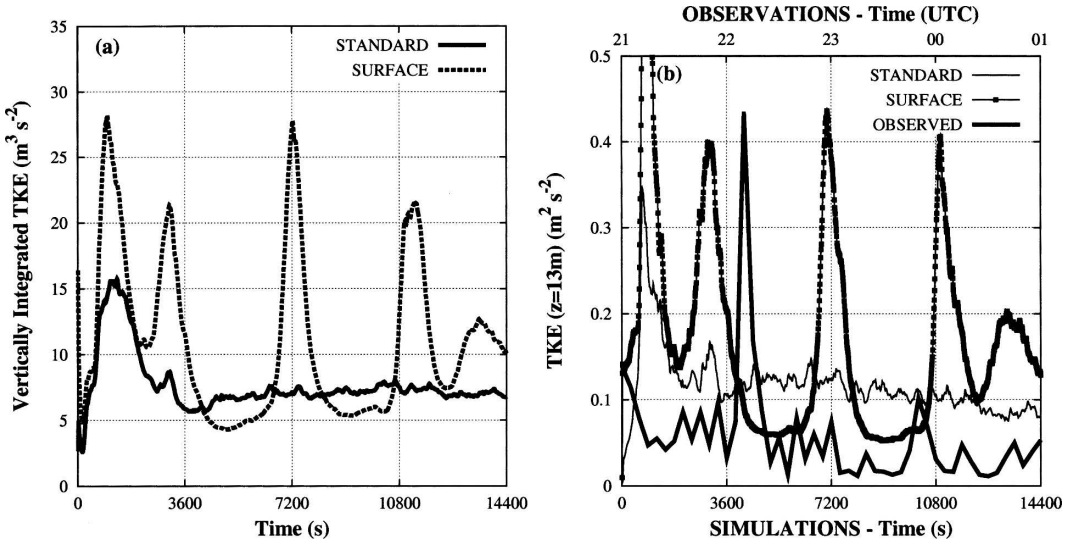

FIG. 6. (a) Vertically integrated TKE time series computed from the standard and the surface-forced runs (see caption Fig. 5). (b) Time series of the TKE at 13 m computed for the two runs and the observed TKE at 13 m from the tower between 2100 and 0100 UTC.

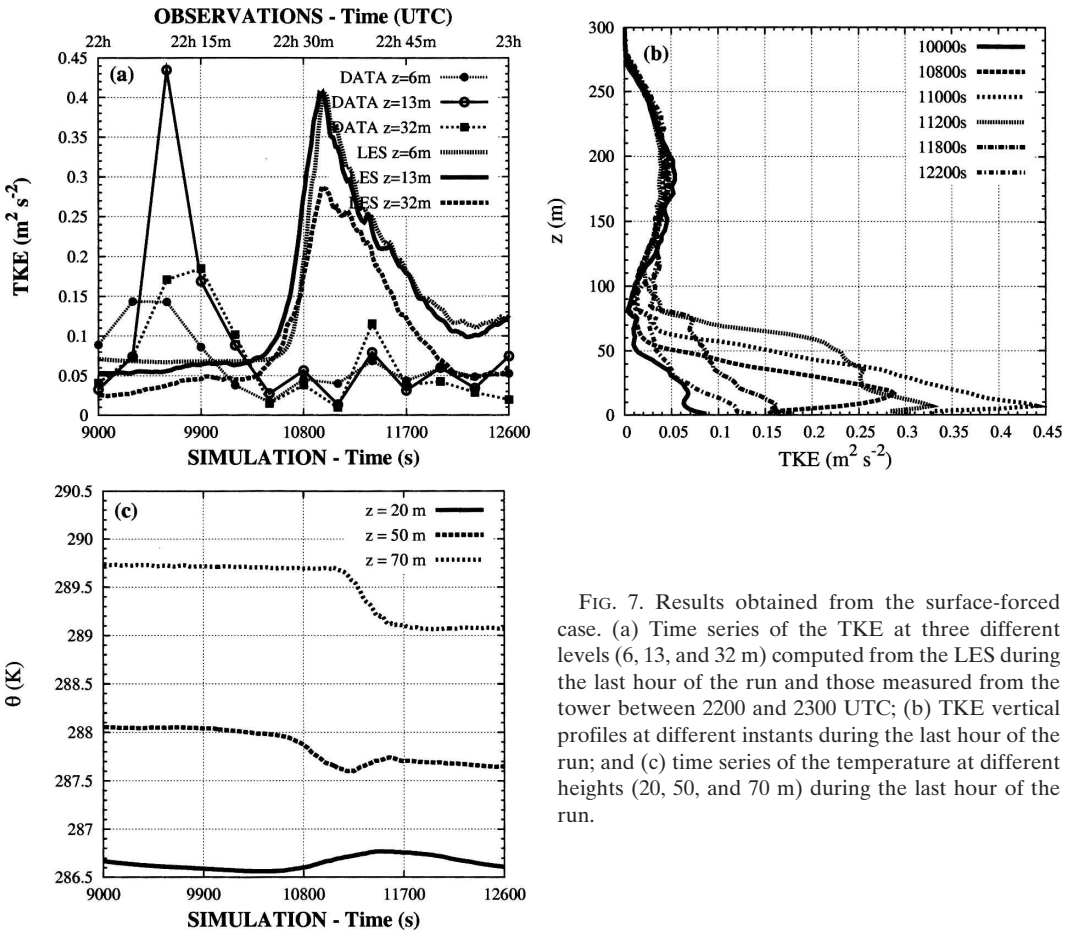

FIG. 7. Results obtained from the surface-forced case. (a) Time series of the TKE at three different levels (6, 13, and 32 m) computed from the LES during the last hour of the run and those measured from the tower between 2200 and 2300 UTC; (b) TKE vertical profiles at different instants during the last hour of the run; and (c) time series of the temperature at different heights (20, 50, and 70 m) during the last hour of the run.

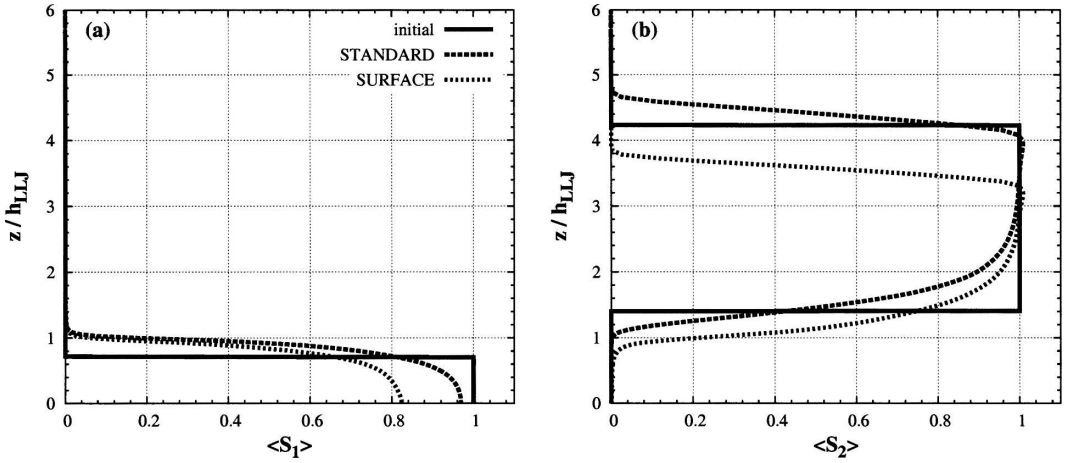

FIG. 8. Averaged scalar concentrations of (a) S_1 and (b) S_2 after 1 h (solid lines) and after 4 h (dotted lines) from the beginning of the run. The y axis is normalized by the LLJ height (h_{LLJ}) obtained for each case.

process. It is clear in Fig. 8a that more scalar is transported across the jet nose upward when the model is forced with observed surface layer conditions. Since this simulation experiences intermittent turbulence, it seems that this procedure is more efficient in transporting mass across the jet that the diffusive-like mixing across the jet nose produced by the standard simulation.

Some more insight can be gained inspecting the temporal evolution of the layer-averaged amounts of scalar. Regarding the transport from below to above the jet (Fig. 9a), the standard simulation has very weak continuous mixing with several bursts not evenly distributed. The forced simulation does not mix continuously across the jet nose but is very efficient in mixing in the oddly distributed turbulent bursts across this level. The mixing from above to the subjet layer (Fig. 9b) shows that it is less efficient than in the other sense, but that it is clearly enhanced in the case of the surface-forced simulation, especially during the turbulence bursts.

In Fig. 10, some diagnostics computed from the LES 1-h statistics are shown that can be interesting for parameterization purposes. The heat and momentum eddy diffusivities (computed dividing the total turbulence flux by the gradient) follow the two-layer pattern, separated by a minimum close to zero at the nose. Note that the values are similar above and below the jet, slightly larger for the heat, and are one order of magnitude smaller than the ones computed for the GABLS first intercomparison case (Beare et al. 2006; Cuxart et al. 2006) for a surface shear-driven moderately stable case. The turbulence Prandtl number is around 0.8 in the upper layer, as found for the GABLS case but var-

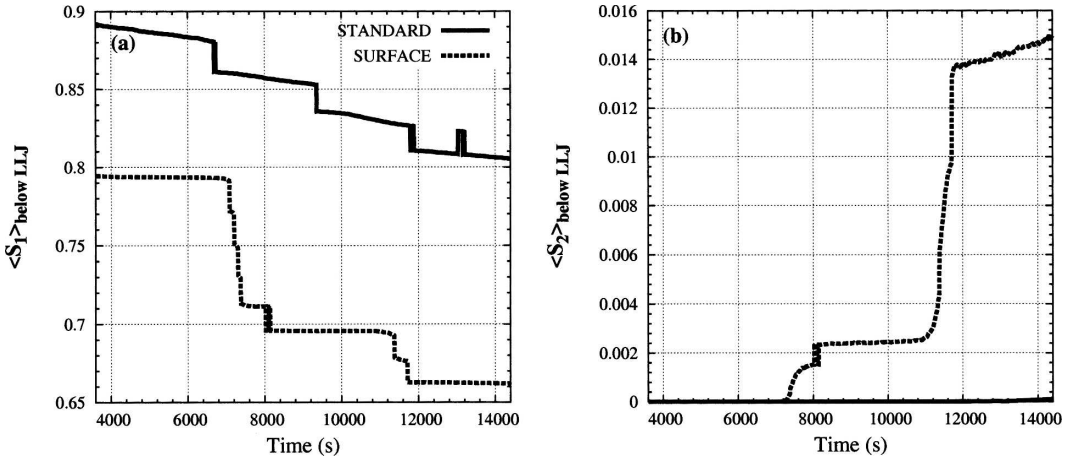

FIG. 9. Time series of the averaged scalar from the ground up to the LLJ height (h_{LLJ}): (a) S_1 and (b) S_2.

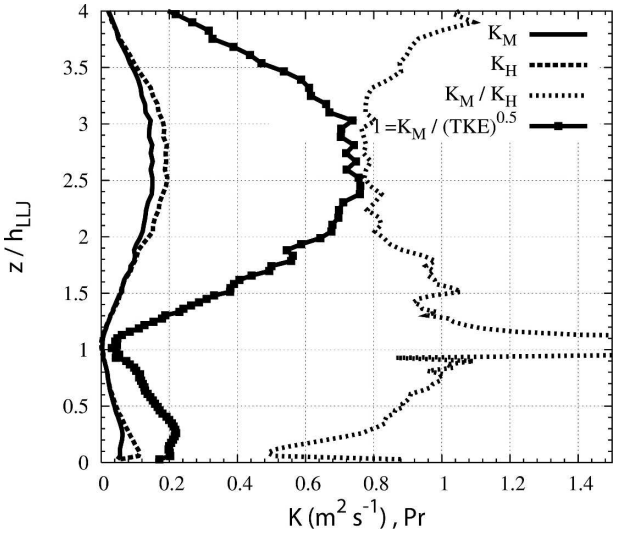

FIG. 10. Eddy diffusivities for heat and momentum (K_H, K_M), turbulence Prandtl number, and mixing length averaged during the fourth hour of the simulation. The y axis is normalized by the LLJ height (h_{LLJ}).

ies a lot with height in the subjet layer. The value at the jet nose has no physical sense.

Some parameterizations prefer to have information about the turbulence scale rather than the mixing coefficient. Here the quotient between the eddy diffusivity for momentum and the square root of the total TKE is plotted. It follows closely the same shape as the eddy diffusivity, but since the TKE is slightly smaller above, the length is larger above than below the jet. The shape is parabolic above the jet with a maximum near 2.5 h_{LLJ}, whereas below the jet the length is the minimum close to the ground and increases with height up to 0.3 h_{LLJ} then decreases with height to almost zero at the jet nose.

6. Comparison of observed and simulated PDFs

Although there were only sonic anemometer measurements up to 32 m, there were more conventional sensors recording at a rate of 5 Hz, up to 50 m for the temperature and up to 100 m for the wind. To see up to what point the LES simulation is realistic beyond the comparison of averaged values, we inspect here the probability density functions (PDFs) measured by those sensors and those produced by the LES at the same levels, the latter computed taking a complete horizontal field every minute during the last hour of the simulation. This comparison will inform if the LES is behaving similarly to the reality or not.

The PDFs for any variable x $[B(x)]$ are normalized such that $\int_{-\infty}^{\infty} B(x)\, dx = 1$, and, to allow for a clear comparison to other series, they are customarily plotted using $\sigma_x B(x')$, where $x' = (x - \overline{x}/\sigma_x)$. Here $\overline{x}$ is the mean value and σ_x is the standard deviation; a log scale is chosen for the y axis to better inspect the tails (Fig. 11). Further explanations are given in Jiménez and Cuxart (2006).

Figure 11a compares the PDFs for the fluctuations of the wind speed at three levels and also to some measurements by Chu et al. (1996) in the stably stratified surface layer. Two different PDFs have been computed from the LES corresponding to the standard run and where the observed surface temperature and wind speed have been imposed (labeled as surface). The LES

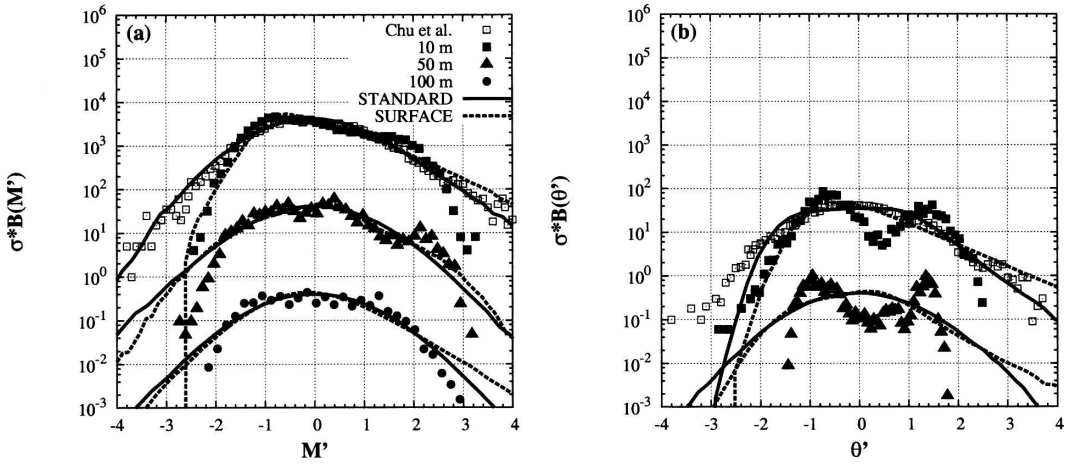

FIG. 11. Normalized PDFs for (a) wind speed and (b) potential temperature computed from data and from the LES (lines) at 10, 50, and 100 m. The PDFs at 50 and 100 m have been shifted up two and four decades, respectively, to clarify the intercomparison. PDFs obtained from data measurements in Chu et al. (1996) are shown by the open squares.

model at 10 m fits better with the Chu et al. (1996) data than the SABLES-98 data. This can be explained by the fact that the Chu et al. data were measured in a classical surface-induced shear-driven SBL, well described by the similarity theory, which is imposed in the first level of the LES model. The data analyzed here, from the SABLES-98 campaign, moderately stable and with a LLJ, most likely do not fulfill the requirements of the standard similarity theory for stable boundary layers, as the PDF tails show. At 50 m, the standard LES generates a quasi-Gaussian distribution, whereas data show asymmetry with the largest values more frequent than the smallest. On the other hand, the PDF of the surface-forced LES has some fluctuations close to the mean value in agreement with the observations. At 100 m, above the wind maximum, the simulations give very similar results and they compare fairly well to the data, although some discrepancies still exist at the tails. This comparison gives support to the idea that the simulation is more realistic above than below the wind maximum.

The fluctuations of temperature at 10 and 50 m are compared in Fig. 11b. In the surface layer, again the LES compares better to the data by Chu et al. than to the present LLJ conditions, supposedly by construction. However, it is very worthy to note here that the observed data show a very clearly defined binormal distribution, both at 10 and at 50 m, with values as significant as ± 0.5 K. The observations could therefore indicate that the mixing below the LLJ maximum is performed either by large eddies, suddenly bringing warmer air to the surface that cools until a new event takes place, or that there could be intrusive bursts from above with a certain periodicity. The standard LES is clearly not able to produce this kind of distribution and acts more as a system immediately reducing any too-large gradient that is formed in the layer. The surface-forced LES introduces some asymmetry but is still far from the observations. The understanding of the PDFs of the observed temperatures needs further investigation.

7. Conclusions

An LES simulation of a LLJ based on field observations has been performed. The model is able to reproduce the observed two-layered structure, consistent in two turbulent layers separated by a change of the temperature gradient very close to the height of the maximum wind speed. The upper-layer characteristics are well captured quite independently on the conditions of the surface, but the results vary significantly in the subjet layer depending on the surface boundary conditions. The radiation is a feature that has to be included in such a study in order to adequately capture the temperature balance close to the surface. However, more resolution would be needed to properly represent the strong temperature gradient near the ground.

The minimum TKE production by wind shear at the jet nose and the fact that the temperature inversion extends up to this layer make it a barrier to the turbulence transport across the layers, being even more stable than the surface layer. The two layers act almost independently but, depending on the configuration of the simulation, can exchange heat and matter, basically through short-lasting turbulence bursts. The modeled bursts are similar to some observed events. The classically averaged LES diagnostics for 1 h do not give trace of this short time-scale mixing and produce a two-layer eddy diffusivity structure that, implemented in a weather or climate model, would not make any transport across the interface.

To progress further in the understanding of the mixing across a LLJ it would be interesting to be able to measure effectively the transport of a passive tracer through the jet nose and evaluate the amount of scalar mixed and the rate at which it is mixed. Of course, the thermal structure of the subjet layer should be better studied, especially when dealing with the values of the turbulence fluxes in the surface layer.

Acknowledgments. Many ideas and comments have arisen in fruitful discussions within the INTERCLE project and also within the GABLS community. We wish to acknowledge them all. The European Centre for Medium-Range Weather Forecasts (Reading, United Kingdom) and the Meso-NH support team are greatly thanked for their computing time and patience. Daniel Martinez (UIB) has processed some SABLES-98 data for the comparison. This work has been partially funded by the research project INTERCLE (REN2002-00486/CLI) of the Spanish Ministry of Research.

REFERENCES

André, J. C., and L. Mahrt, 1982: The nocturnal surface inversion and influence of clear-air radiative cooling. *J. Atmos. Sci.,* **39,** 864–878.

Banta, R. M., R. K. Newsom, J. K. Lundquist, Y. L. Pichugina, R. L. Coulter, and L. Mahrt, 2002: Nocturnal low-level jet characteristics over Kansas during CASES-99. *Bound.-Layer Meteor.,* **105,** 221–252.

——, Y. L. Pichugina, and R. K. Newsom, 2003: Relationship between low-level jet properties and turbulence kinetic energy in the nocturnal stable boundary layer. *J. Atmos. Sci.,* **60,** 2549–2555.

Beare, R. J., and Coauthors, 2006: An intercomparison of large-

eddy simulations of the stable boundary layer. *Bound.-Layer Meteor.,* **118,** 247–272.

Blackadar, A. K., 1957: Boundary layer wind maxima and their significance for the growth of nocturnal inversions. *Bull. Amer. Meteor. Soc.,* **38,** 283–290.

Bonner, W. D., 1968: Climatology of the low-level jet. *Mon. Wea. Rev.,* **96,** 833–850.

Businger, J. A., 1973: Turbulent transfer in the atmospheric surface layer. *Workshop on Micrometeorology,* D. A. Haugen, Ed., Amer. Meteor. Soc, 67–100.

Chu, C. R., M. B. Parlange, G. G. Katul, and J. D. Albertson, 1996: Probability density functions of turbulent velocity and temperature in the atmospheric surface layer. *Water Resour. Res.,* **32,** 1681–1688.

Conangla, L., and J. Cuxart, 2006: On the turbulence in the upper part of the low-level jet: An experimental and numerical study. *Bound.-Layer Meteor.,* **118,** 379–400.

Cuxart, J., and Coauthors, 2000a: Stable Atmospheric Boundary-Layer Experiment in Spain (SABLES-98): A report. *Bound.-Layer Meteor.,* **96,** 337–370.

——, P. Bougeault, and J.-L. Redelsperger, 2000b: A turbulence scheme allowing for mesoscale and large-eddy simulations. *Quart. J. Roy. Meteor. Soc.,* **126,** 1–30.

——, and Coauthors, 2006: Single-column model intercomparison for a stably stratified atmospheric boundary layer. *Bound.-Layer Meteor.,* **118,** 273–303.

——, M. A. Jiménez, and D. Martínez, 2007: Nocturnal katabatic and mesobeta basin flows on a midlatitude island. *Mon. Wea. Rev.,* **135,** 918–932.

Deardorff, J. W., 1980: Stratocumulus-capped mixed layers derived from a three-dimensional model. *Bound.-Layer Meteor.,* **18,** 495–527.

Derbyshire, S. H., 1990: Nieuwstadt's stable boundary layer revisited. *Quart. J. Roy. Meteor. Soc.,* **116,** 127–158.

Gal-Chen, T., and R. C. J. Somerville, 1975: On the use of a coordinate transformation for the solution of the Navier-Stokes equations. *J. Comput. Phys.,* **17,** 209–228.

Garratt, J. R., and R. A. Brost, 1981: Radiative cooling effects within and above the nocturnal boundary layer. *J. Atmos. Sci.,* **38,** 2730–2746.

Gopalakrishnan, S. G., M. Sharan, R. T. McNider, and M. P. Singh, 1998: Study of radiative and turbulent processes in the stable boundary layer under weak wind conditions. *J. Atmos. Sci.,* **55,** 954–960.

Ha, K.-J., and L. Mahrt, 2003: Radiative and turbulent fluxes in the nocturnal boundary layer. *Tellus,* **55A,** 317–327.

Jiménez, M. A., and J. Cuxart, 2005: Large-eddy simulations of the Stable Boundary Layer using the standard Kolmogorov theory: Range of applicability. *Bound.-Layer Meteor.,* **115,** 241–261.

——, and ——, 2006: Study of the probability density functions from a large-eddy simulation of a stably stratified case. *Bound.-Layer Meteor.,* **118,** 401–420.

Lafore, J. P., and Coauthors, 1998: The Meso-NH Atmospheric Simulation System. Part I: Adiabatic formulation and control simulations. *Ann. Geophys.,* **16,** 90–109.

Lenschow, D. H., X. S. Li, C. J. Zhu, and B. B. Stankov, 1988: The stably stratified boundary layer over the Great Plains. I. Mean and turbulence structure. *Bound.-Layer Meteor.,* **42,** 95–121.

Lipps, F. B., and R. S. Hemler, 1982: A scale analysis of deep moist convection and some related numerical calculations. *J. Atmos. Sci.,* **39,** 2192–2210.

Mahrt, L., R. C. Heald, D. H. Lenschow, B. B. Stankov, and I. B. Troen, 1979: An observational study of the structure of the nocturnal boundary layer. *Bound.-Layer Meteor.,* **17,** 247–264.

——, J. Sun, W. Blumen, T. Delany, and S. Oncley, 1998: Nocturnal boundary-layer regimes. *Bound.-Layer Meteor.,* **88,** 255–278.

Morcrette, J.-J., 1990: Impact of changes to the radiation transfer parameterizations plus cloud optical properties in the EC-MWF model. *Mon. Wea. Rev.,* **118,** 847–873.

Poulos, G. S., and Coauthors, 2002: CASES-99: A comprehensive investigation of the stable nocturnal boundary layer. *Bull. Amer. Meteor. Soc.,* **83,** 555–581.

Räisänen, P., 1996: The effect of vertical resolution on clear-sky radiation calculations: Tests with two schemes. *Tellus,* **48A,** 403–423.

Smedman, A. S., M. Tjernström, and U. Högström, 1993: Analysis of the turbulence structure of a marine low-level jet. *Bound.-Layer Meteor.,* **66,** 105–126.

Stull, R. B., 1988: *An Introduction to Boundary Layer Meteorology.* Kluwer Academic, 666 pp.

Tjemkes, S. A., and P. G. Duynkerke, 1989: The nocturnal boundary layer: Model calculations compared with observations. *J. Appl. Meteor.,* **28,** 161–175.

Van de Wiel, B. J. H., R. J. Ronda, A. F. Moene, H. A. R. De Bruin, and A. A. M. Holtslag, 2002: Intermittent turbulence and oscillations in the stable boundary layer over land. Part I: A bulk model. *J. Atmos. Sci.,* **59,** 942–958.

Whiteman, C. D., X. Bian, and S. Zhong, 1997: Low-level jet climatology from enhanced rawinsonde observations at a site in the southern Great Plains. *J. Appl. Meteor.,* **36,** 1363–1376.

Wyngaard, J. C., and R. A. Brost, 1984: Top-down and bottom-up diffusion of a scalar in the convective boundary layer. *J. Atmos. Sci.,* **41,** 102–112.